Received: 17 April 2020 | Revised: 8 June 2020 | Accepted: 14 June 2020

DOI: 10.1002/app.49704

ARTICLE

Applied Polymer SCIENCE WILEY

Low-cycle fatigue behavior of flexible 3D printed thermoplastic polyurethane blends for thermal energy storage/release applications

Daniele Rigotti[1,2] | **Andrea Dorigato**[1,2] | **Alessandro Pegoretti**[1,2]

[1]Department of Industrial Engineering, University of Trento, Trento, Italy

[2]National Interuniversity Consortium of Materials Science and Technology (INSTM), Florence, Italy

Correspondence
Daniele Rigotti and Alessandro Pegoretti, Department of Industrial Engineering, University of Trento, Via Sommarive 9, Trento 38123, Italy.
Email: daniele.rigotti-1@unitn.it (D. R.) and alessandro.pegoretti@unitn.it (A. P.)

Abstract

Thermal energy storage (TES) materials constituted by a microencapsulated paraffin having a melting temperature of 6°C and a thermoplastic polyurethane (TPU) matrix were prepared through fused deposition modeling. Scanning electron microscope (SEM) micrographs demonstrated that the microcapsules were homogeneously distributed within the matrix, with a rather good adhesion within the layers of 3D printed specimens, even at elevated concentrations of microcapsules. The presence of paraffin capsules having a rigid polymer shell lead to a stiffness increase, associated to a decrease in the stress and in the strain at break. Tensile and compressive low-cycles fatigue tests showed that the presence of microcapsules negatively affected the fatigue resistance of the samples, and that the main part of the damage occurred in the first fatigue cycles. After the first 10 loading cycles at 50% of the stress at break, a decrease in the elastic modulus ranging from 60% for neat TPU to 80% for composite materials was detected. This decrease reached 40% of the original value at 90% of the stress at break after 10 cycles. Differential scanning calorimetry tests on specimens after fatigue loading highlighted a substantial retention of the original TES capability, in the range of 80%–90% of the pristine value, even after 1000 cycles, indicating that the integrity of the capsules was maintained and that the propagation of damage during fatigue tests took probably place within the surrounding polymer matrix. It could be therefore concluded that it is possible to apply the developed blends in applications where the materials are subjected to cyclic stresses, both in tensile and compressive mode.

KEYWORDS

applications, elastomers, mechanical properties, thermal properties

1 | INTRODUCTION

The practice of running has increased popularity worldwide in the last 30 years and it was followed by an increasing interest of the scientific community toward the biomechanical aspects of this sport activity.[1] The shoes represent the contact point between the athlete and the surface, so they play a key role in determining the running efficiency. Therefore, the issues related to the material selection in sport shoes are becoming more and more important, and this choice must be tailored to the particular activity, which the item is aimed for.[2] As

reported by Nigg et al.,[3] the mechanical properties of material utilized for the running shoes influence the specific oxygen consumption, the intensities of muscle activation, and the wavelet frequencies of the electromyogram (EMG) signals. A study of Chen et al.,[4] indicated that adapting the stiffness of the materials used in different parts of the shoes is necessary to provide an optimal energy return at specific running conditions.

Polymeric foams are commonly used in shoes industry as a midsole shock-absorbing material, and the vast majority of the insoles for running applications are made of ethylene vinyl acetate (EVA). However, thermoplastic polyurethanes (TPUs) present superior properties in terms of mechanical resistance and fatigue performances. In this sense, some efforts were made to demonstrate that TPU foams could successfully replace EVA in the midsole section of the shoes, because of the better impact damping properties.[5] TPUs are characterized by a limited stiffness and an elevated strain at failure.[6] Therefore, TPU has intermediate properties between rubber and hard thermoplastics, it can be plastically deformed upon heating, showing elevated elasticity and adhesion without sticking as rubbers. Differently to common cross-linked elastomers, thermoplastic elastomers (TPEs) have weak secondary chemical bonds (i.e., hydrogen bonds) and thus they can be remelted.[7,8] Moreover, their mechanical properties are determined by the relative concentration of hard and soft segments within the main chain.[9] Because of these peculiar properties, TPUs were the first TPEs used and their main applications were automotive exterior parts and shoe soles.[9] In particular, TPUs are applied as covering material to improve the protection in the lateral area of trail running shoes, where the possibility to hit rocks is higher, as rigid inserts to improve the compatibility with external items such as crampons in mountaineering boots or to incorporate inside the shoes rigid structures to improve the support of the ankle articulation.

Considering the intended application of TPUs as shock-absorbing materials for running shoes, it is clear that the characterization of their fatigue behavior has a fundamental role. In fatigue tests on TPUs it was generally observed that the failure of the components at elevated testing cycles is generally associated to a localized increase of the temperature, but it is important to point out that this effect in low to moderate cyclic loads, that are characteristic of walking and running activities, is not so pronounced.[10] Moreover, also the manufacturing technique of TPU components strongly affects their fatigue performances. In fact, the thermoplastic nature of TPU allows this material to be processed by additive manufacturing (AM), combining thus an excellent tear and wear resistance with elevated impact strength and flexibility.[11] In particular, TPU can be successfully applied in AM technologies such as fused deposition modeling (FDM). FDM technique, commonly known as 3D printing, represents one of the most widespread AM technologies. In FDM, components are constructed by depositing strands or beads of molten polymer layer-by-layer. The insertion of fillers with specific properties and/or the blending of different materials offer the possibility to produce high-performance 3D printable composites with improved properties. Applications where this technology has already proven efficient include: biomedical, mechanical, electrical, thermal, and optically enhanced products.[12] Due to their thermoplastic-like processability and unique elasticity, TPEs have gained much attention among the various materials for FDM.[13–16] In this sense, TPU offers the possibility to produce tailorable and flexible cellular structures to be applied in specific energy-absorbing parts.[17] Several studies were carried out to correlate the main manufacturing parameters of 3D printed specimens and their fatigue life, and it was evidenced that both the infill density[18] and the build orientation[19] significantly affect their fatigue behavior. Senatov et al.[20] demonstrated that a reduction of the modulus of elasticity was followed by an increase of the cyclic stress in porous PLA scaffolds obtained through FDM. In that work, the stiffness degradation during cyclic fatigue loading was found to be caused by multiple damage modes and followed a three-stage progression similar to that of composite materials. The main part of the damage took place in the first cycles of the test due to crazing, fiber cracking, and delamination, while the decrease of elastic modulus till the final fracture was due to the collapse of the printed structure and due to the accumulation of microdamages.[21]

In sport applications, thermal energy storage (TES) technologies are mainly used in the textile industries to provide thermal comfort to the athletes. TES materials are multifunctional systems able to store heat through the heating of a medium, with the aim to utilize (release) the stored energy when required (on cooling).[22] It is therefore possible to apply TES technology to produce "smart" fabrics able to keep constant the temperature of the body.[23] In particular, latent heat TES systems possess an elevated energy storage density at the transition temperature of the phase change material (PCM), and for this reason, they received much attention by the researchers. In PCMs, a solid/liquid or a solid/solid transition is generally involved, and they can be classified as organic, inorganic or eutectic alloys.[24–26] PCMs having solid–liquid transitions, typical of paraffins, are perhaps the most widely applied. Paraffins derive from petroleum cuts and are endowed with good chemical and thermal stability, and limited vapor pressure. These materials are

able to store a considerable amount of latent heat, available with a limited super-cooling and with good reliability (i.e., they have stable TES capability for 1000–2000 cycles). The most important drawbacks related to the use of paraffins is represented by their limited thermal conductivity (around 0.2 $W \cdot m^{-1} K^{-1}$),[27] and their leakage at the molten state,[28],[29].[30] One the most common solutions to limit the problem of the leakage is the micro-/nano-encapsulation of the paraffin inside a polymeric or inorganic shell.[31–34] Therefore, PCM can help thermoregulation of human body in competitions characterized by extremely hot or cold temperatures,[35] as commonly happens in winter sports like skiing, skating, bobsledding, and so on. In the same way, PCM can be also incorporated in winter sport clothes in order to release heat when the external temperature decreases. Cooling could be useful in summer sports, such as marathons or bike races. The TES efficiency provided by PCMs is strongly influenced by many factors, such as the concentration of PCM within the matrix, the area and the part on the human body covered by PCM.[36] In a previous work of our group multifunctional TES materials were prepared by encapsulating a paraffin having a melting temperature of 6°C in a TPU matrix, and the most important thermomechanical properties of the resulting samples were investigated.[37] The same materials were then utilized to develop 3D printable TPU blends with TES capabilities. In this work, different loadings of an encapsulated paraffin were added to a TPU matrix, and the resulting blends were then utilized to produce 3D printed samples that could be potentially used for the production of insoles for winter sports applications.[38]

If the PCM microencapsulation represents an efficient way to stabilize paraffin within a polymer matrix, no comprehensive studies are nowadays present in literature on the behavior of the microencapsulated paraffin subjected to mechanical fatigue cycles.[35] Only Casado et al.[10] tried to correlate the fatigue life of a composite based on a glass fiber reinforced thermoplastic PA6,6 in which hydrated salts were added as PCM. They evidenced that the addition of PCM can produce a cooling effect on the thermoplastic matrix capable of controlling the viscoelastic processes that promotes the temperature enhancement of the polymer exposed to cyclic loads, with beneficial effects on the fatigue life of the material.[10] However, the effect of the cyclic loadings on the structural integrity and on the retention of the TES capability of the capsules has been never studied in literature.

Therefore, the purpose of the present study is to investigate the thermal and mechanical behavior at low-fatigue cycles of polymer blends in which microcapsules with a low-melting point paraffin ($T_m = 6°C$) were dispersed in a commercial TPU matrix. The resulting blends were then 3D printed using FDM technology. The outcomes of this work represent a complementary part of a wider research activity aimed at developing 3D printable materials with thermal energy management capability, to be utilized for winter sport applications.

2 | MATERIALS AND METHODS

2.1 | Materials

TPU pellets of Desmopan 6064A, having a density of 1.09 g/cm^3 and a melting temperature of 200°C, were kindly provided by Covestro Srl (Milano, Italy). This is an injection-molding grade TPU that finds application in automotive interior and shoe soles, because of its excellent mechanical properties and microbial resistance, low abrasion and the absence of plasticizers. A microencapsulated paraffin Microtek MPCM6D (named M6D in this work), purchased from Microtek Laboratories Inc. (Dayton, OH, USA), was used as PCM. These melamine formaldehyde microcapsules contain a paraffin wax with a melting temperature (T_m) of 6°C and a crystallization temperature (T_c) of about −10°C. The microcapsules have a mean size of 17–20 μm, a density of 0.9 g/cm^3, and are constituted by 85–90 wt% of paraffin. According to the datasheet, their melting enthalpy is in the range 157–167 J/g.

2.2 | Filament extrusion

TPU granules were finely grinded and mixed with the microcapsules using a mechanical stirrer to avoid the leakage of paraffin from the capsules. The resulting powder was then extruded through an Estru13 single screw extruder, supplied by Friul Filiere SpA (Udine, Italy), having a screw diameter of 14 mm and an extrusion head of 3.0 mm. A screw speed of 30 rpm and a temperature profile from 105°C (feeding section) to 180°C (die zone) were set. With this temperature profile, it was possible to optimize the surface quality and to avoid porosity inside the filaments. In this way, filaments with a constant diameter of about 1.75 ± 0.10 mm were obtained. Basing on the results obtained in previous works of our group,[37,38] neat TPU samples and blends with a microcapsules content of 30 wt% (TPU_30M6D) and 40 wt% (TPU_40M6D) were prepared.

2.3 | 3D printed samples preparation

The 3D printed specimens were produced from the extruded filaments by using a Sharebot Next Generation desktop 3D printer. In this research two types of

specimens were printed: a dog bone specimen type 1BA according to ISO527 for tensile tests, and a cylinder with a diameter of 30 mm and a height of 10 mm, to be utilized for compression tests. These specimens were designed by using SolidWorks software, the 3D models were then exported in a. STL format, processed by Slicer and exported in a GCODE format. A rectangular infill with a density of 100% was selected, while the infill angle was set in configuration 0°/0°, to maximize the density and the mechanical properties of the resulting samples. Considering that increasing the percentage of microcapsules inside the TPU matrix made the printing stage more difficult, a feeding configuration with a 0° angle resulted the best choice for the preparation of the printed materials. After a process optimization, the following parameters were selected for the 3D printing: layer height 0.20 mm, nozzle temperature 240°C, bed temperature 40°C, deposition rate 40 mm/s. The cylindric specimens for compression test were printed with a honeycomb structure with an infill density of about 25% that resembles the structure present in some high-level sports shoes. In Figure 1(a,b) representative images of the 3D printed dumbbell specimens and of the cylinders for the compression test are reported. The neat matrix was denoted as TPU, while the blends were designed indicating the matrix and the weight percentage of PCM. For instance, TPU_30M6D indicates the polymer blend with the 30 wt % of microcapsules.

2.4 | Experimental techniques

Microstructural images of the cryo-fractured surfaces of the 3D printed samples were taken in order to investigate the efficiency of the printing process and the surface interaction between microcapsules and the TPU matrix. A Zeiss Supra 40 field emission scanning electron microscope (FESEM), operating at an accelerating voltage of 2.5 kV, was utilized. A thin platinum palladium conductive coating was deposited on the surface of the samples before the observations.

Differential scanning calorimetry (DSC) tests were carried out through a Mettler Toledo DSC30 calorimeter, testing samples of about 10 mg under a nitrogen flow of 150 ml/min. A first heating run from −100 to 220°C was followed by a cooling stage from 220°C to −100°C and by a second heating stage until 220°C. All these scans were carried out at 10°C/min. The melting (T_m), the crystallization (T_c) temperatures were determined from the endothermic and exothermic peaks, while the glass transition temperature (T_g) was assessed from the inflection point. From the area under the exothermic peak it was possible to estimate the specific enthalpy of crystallization (ΔH_c), while from and area under endothermic peak the specific enthalpy of melting (ΔH_m) was determined.

The mechanical properties of the resulting samples were analyzed through quasi-static tensile tests at room temperature. These tests were performed on 3D printed dumbbell specimens according to ASTM D638 standard, by using an Instron 5969 universal tensile testing machine, equipped with a load cell of 50 kN, operating at a testing speed of 100 mm/min. An Instron Mod. 2603–080/656 long-travel extensometer was utilized to detect the deformation during the tensile tests. Five specimens were tested for each composition, and in this way, it was possible to determine the chord modulus at a deformation of 10%, the stress at break (σ_b) and the strain at break (ε_b).

Fatigue tests in tensile mode were carried out to investigate the trend of the most mechanical properties of 3D printed samples subjected to a cyclic load, in order to understand also the fatigue limit of these kind of materials. An Instron 5969 machine, equipped with a load cell of 50 kN, was utilized. A triangular fatigue stress profile was utilized, adopting a crosshead speed of 10 mm/min (see Figure 2).

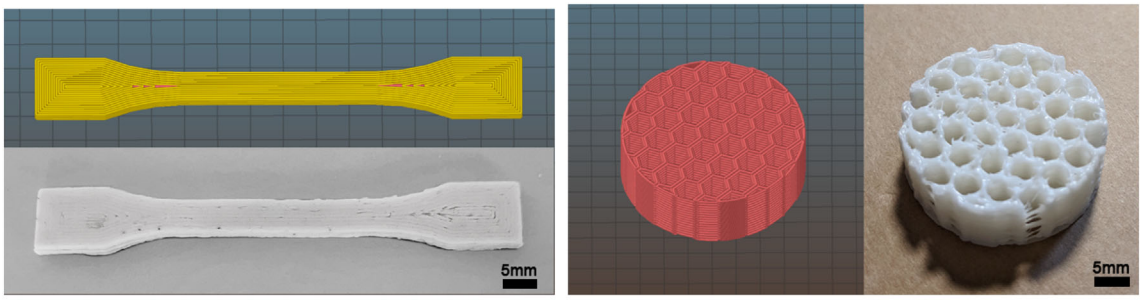

FIGURE 1 Representative images of (a) 3D printed dumbbell specimen and (b) 3D printed compression specimen [Color figure can be viewed at wileyonlinelibrary.com]

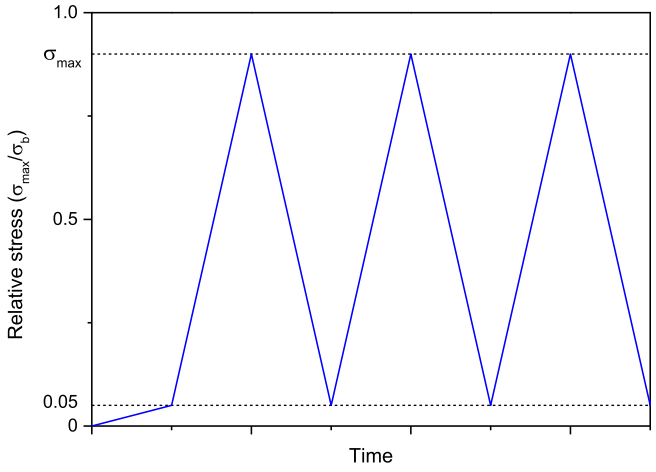

FIGURE 2 Representative stress-time profile applied in fatigue tests in tensile mode [Color figure can be viewed at wileyonlinelibrary.com]

Specimens were prestressed at 0.05 MPa in tensile mode and pulled to a specific fraction of the stress at break measured in quasi-static tensile tests. After 1000 cycles (or after the breakage of the specimens in case of premature failure) the test was stopped and about 10 mg of material was extracted from the area near the rupture to perform DSC test. In this way, it was possible to evaluate the retention of the TES capability of the tested samples after repeated fatigue cycles. Compression fatigue tests allowed to extract a small specimen for DSC test after a precise number of fatigue cycles, in order to test the TES efficiency of the materials as a function of the fatigue cycles, without compromising the resistant section of the cylinder. This approach was not applicable in tensile tests, and the specimens for DSC analysis were extracted only after the breakage of the samples. Moreover, compression test allowed to impart a higher stress to the microcapsules, evaluating thus their resistance in a harsher mechanical environment. The shape of the fatigue profile utilized in compression tests was similar to that depicted in Figure 2, but in this case the preload was set at 0.01 MPa, and two maximum stress levels were adopted (i.e., 0.1 MPa and 0.5 MPa). These stress levels were selected because they could be significative to reproduce a pressure inside the shoes in real conditions during a low and a high-intensity activity, respectively.[39]

3 | RESULTS AND DISCUSSIONS

3.1 | Morphological features

Considering that the thermomechanical properties of prepared materials are strictly connected to their morphological features, the microstructure of the cryo-fractured sections of 3D printed samples of TPU_30M6D and TPU_40M6D was investigated by FESEM, and the most representative micrographs are reported in Figure 3(a,b). Macroscopic triangular holes can be detected in correspondence of the edges of the pristine filaments, but no welding lines are visible between layers, meaning that a good adhesion was achieved. On the surface, it is possible to notice the presence of capsules with dimensions ranging from 10 to 20 μm. No microcapsules agglomerates can be detected and uniform distribution of M6D could allow to retain the morphological continuity of the matrix even at elevated M6D concentrations. This feature could positively affect the mechanical and fatigue behavior of the resulting blends.

3.2 | Quasi-static tensile behavior

In Table 1 the most important mechanical parameters obtained from quasi-static tensile tests on the 3D printed samples are summarized (representative stress–strain curves on similar systems can be found in Reference 38). The addition of microcapsules promotes a stiffening of the materials accompanied by an evident embrittlement of the samples. In fact, the elastic modulus passes from 4.9 MPa for the neat TPU up to 9.8 MPa for the TPU_40M6D. As already reported in our previous works on bulk TPU/microcapsules blends, it can be hypothesized that the observed modulus increase is due to the higher elastic modulus of the capsules with respect to that of the TPU matrix.[37] The observed stiffness increase comes at the expenses of the failure properties, and in fact a drastic reduction of the stress at break, of the strain at break and of the absorbed energy was observed even at a M6D amount of 30 wt%. The observed reduction of the failure properties probably indicates that the adhesion between the M6D shell and the TPU matrix should be improved. In these conditions, the TPU/microcapsules interface represents a high-stress concentration point where the nucleation of microcracks is promoted, leading to a premature failure the material.

In order to gain a deeper insight on the elastic properties of the investigated materials, the dependence of the elastic modulus of the investigated materials was modeled as a function of the composition. In particular, the elastic modulus of the 3D printed samples was modeled through the Halpin-Tsai empirical model, which represents a useful approach to model the stiffness of composites as a function of the filler concentration and aspect ratio.[40] According to this model, the tensile modulus of a particulate filled polymer composite (E_c) can the determined through the expressions reported in Equations (1) and (2):

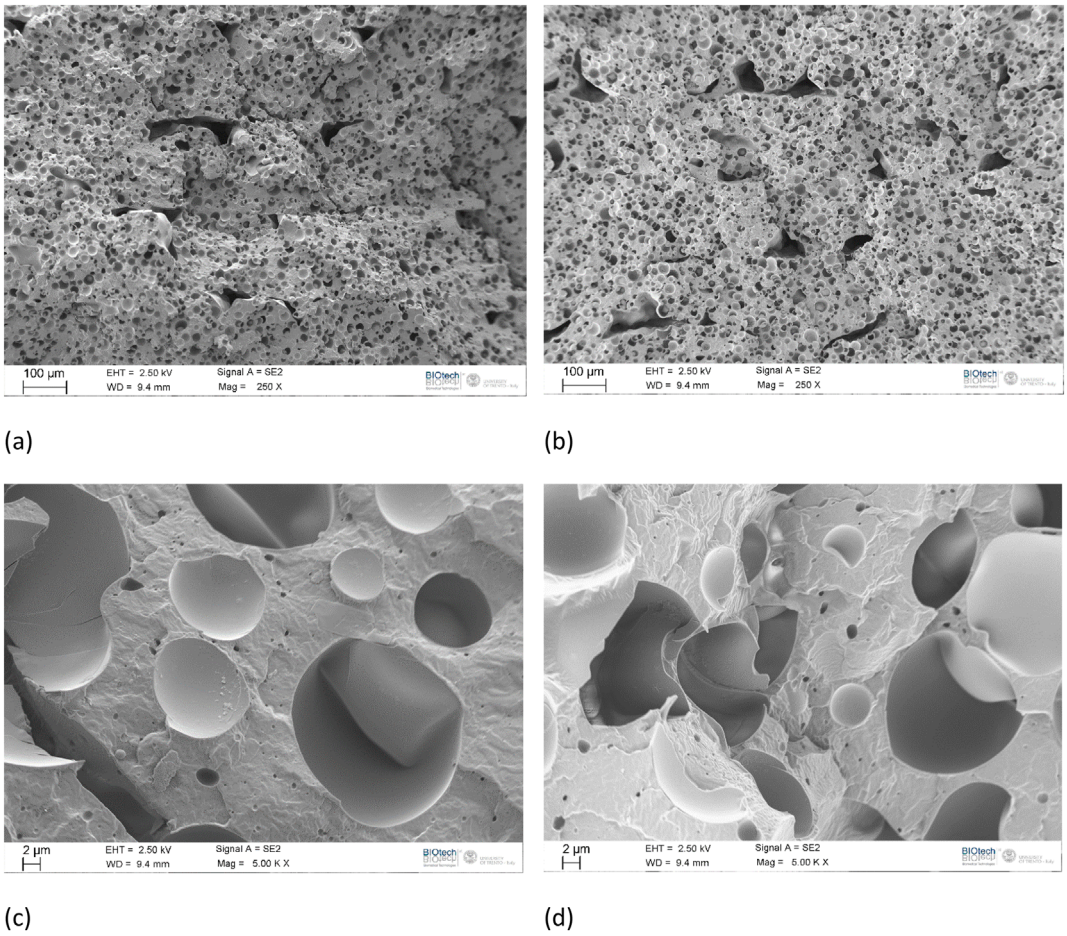

FIGURE 3 Low magnification SEM micrographs of 3D printed (a) TPU_30M6D and (b) TPU_40M6D samples. Higher magnification of (c) TPU_30M6D and (d) TPU_40M6D samples. SEM, scanning electron microscope; TPU, thermoplastic polyurethane [Color figure can be viewed at wileyonlinelibrary.com]

TABLE 1 Results from quasi-static tensile tests on the prepared blends

	Chord modulus (MPa)	Stress at break (MPa)	Strain at break (mm/mm)	Energy at break (J/mm^2)
TPU	4.9 ± 0.4	7.9 ± 0.3	9.8 ± 0.6	1.23 ± 0.09
TPU_30M6D	8.4 ± 0.7	1.5 ± 0.2	4.2 ± 0.1	0.14 ± 0.02
TPU_40M6D	9.5 ± 0.5	0.9 ± 0.1	4.2 ± 0.1	0.09 ± 0.01

Abbreviation: TPU, thermoplastic polyurethane.

$$E_c = E_m \frac{1 + 2\eta V_f}{1 - \eta V_f}, \quad (1)$$

$$\eta = \frac{\frac{E}{E_m} - 1}{\frac{E_f}{E_m} + 2}, \quad (2)$$

where E_f and E_m are, respectively, the elastic modulus of the filler (unknown) and of the matrix (4.9 MPa). In Figure 4, elastic modulus data of the samples are fitted with Halpin-Tsai model. Applying a least square minimization procedure, it was possible to determine the best fitting curve by imposing a microcapsule elastic modulus of 20.6 ± 1.7 MPa. Even if this value is slightly lower than that detected in our previous work of bulk TPU/M6D blends (28.4 MPa),[37] this discrepancy is not so pronounced, and it could be partly attributed to the presence of pores within the 3D printed structures. In fact, from pycnometric measurements it was found that the means porosity degree for all the prepared material is around 32%.

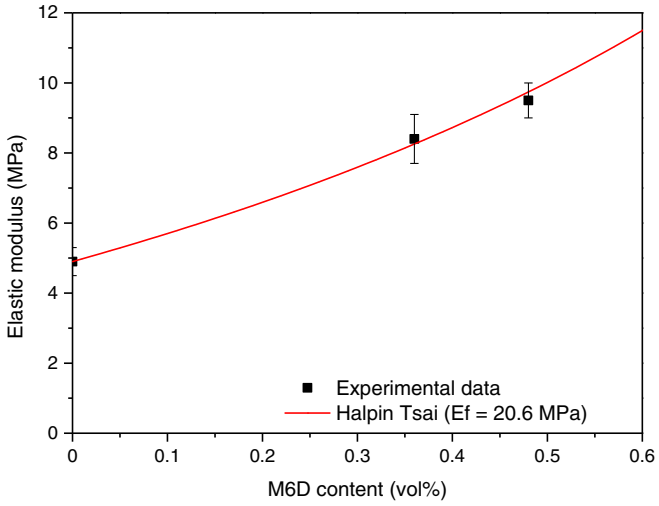

FIGURE 4 Fitting of elastic modulus data of the prepared blends with Halpin-Tsai model—Equation (1) [Color figure can be viewed at wileyonlinelibrary.com]

3.3 | Tensile fatigue tests

In Figure 5(a–d) are shown the representative stress–strain curves of 3D printed TPU_30M6D sample at different fatigue cycles, with a maximum applied fatigue stress (σ_{max}) equal to 30%, 50%, 70%, and 90% of the stress at break (σ_b) detected in quasi-static tensile tests. The same curves were obtained also for the 3D printed specimens made of neat TPU and TPU_40M6D, but they were not presented for sake of brevity. According to Figure 5, it is evident that the stiffness of the samples decreases with the number of fatigue cycles at all stress levels, meaning that a progressive damage evolution within the material occurs. Analyzing the hysteresis loops it is possible to observe that the greatest part of the absorbed energy is related to the first fatigue cycle, regardless to the maximum stress. This means that most of the damage within the sample occurs in the first stages of the fatigue tests.

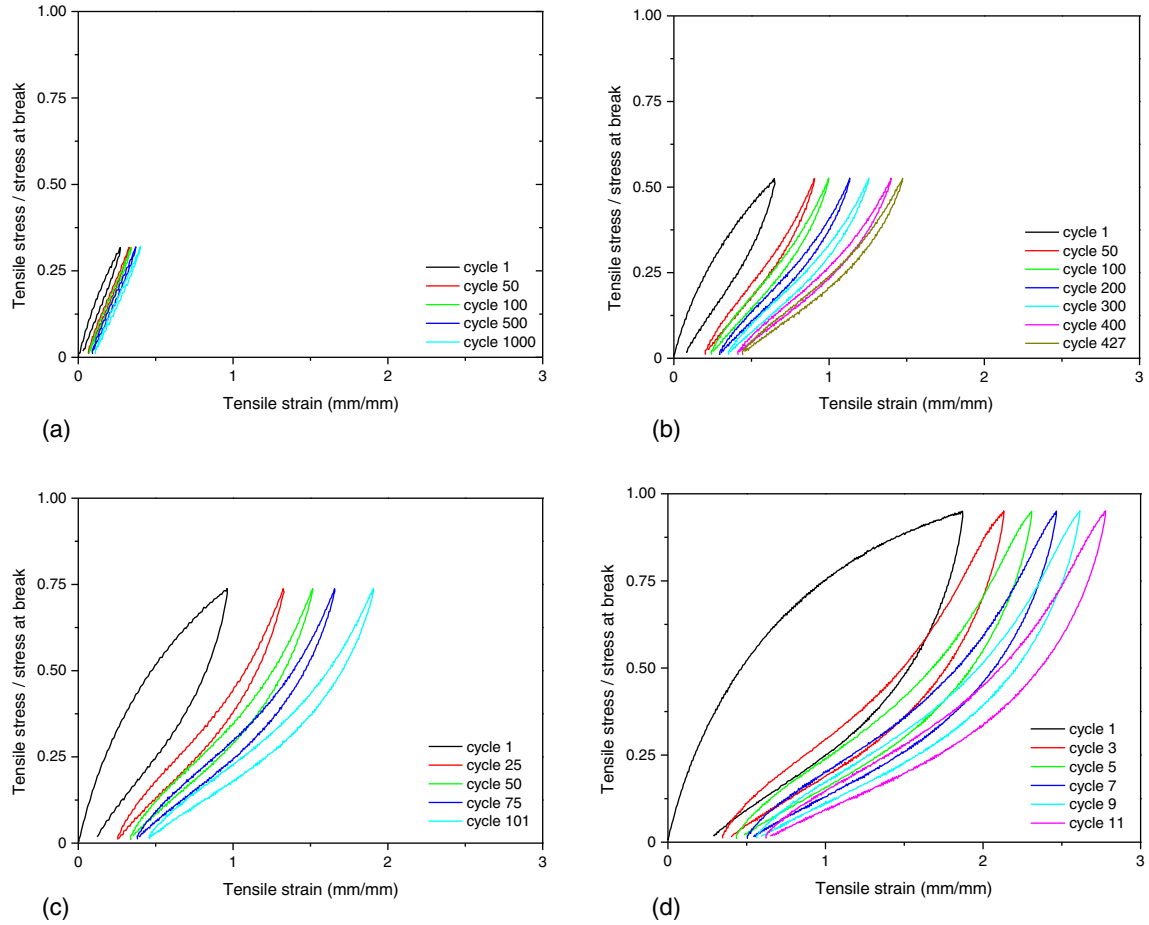

FIGURE 5 Hysteresis curves from tensile fatigue tests on TPU_30M6D sample tested applying a maximum stress equal to the (a) 30%, (b) 50%, (c) 70%, and (d) 90% of the stress at break. TPU, thermoplastic polyurethane [Color figure can be viewed at wileyonlinelibrary.com]

From the Wohler curves reported in Figure 6, it can be seen that neat TPU sample breaks after 70 cycles at a fatigue stress equal to the 90% of the stress at break, while for lower stress levels the breakage was not achieved within 1000 cycles. It can be concluded that TPU sample shows a rather good fatigue resistance and that the failure of this material under fatigue loadings occurs only at stress levels approaching to the stress at break. Considering that fatigue curves of the M6D filled materials, it can be seen that microcapsules addition determines a considerable lowering of the fatigue resistance. In fact, TPU_40M6D sample breaks at a stress equal to 0.5 σ_b after 380 cycles, while for the TPU_30M6D blend the failure occurs at the same stress level after 100 cycles. For both materials the failure was not detected within 1000 testing cycles for an applied stress of 0.5 σ_b. Once again, the lowering of the fatigue resistance upon M6D addition could be explained by the nonoptimal interfacial adhesion between the capsules and the TPU matrix. TPU_40M6D sample shows better fatigue performances with respect to the blend with a microcapsules content of 30 wt%. Considering the results of quasi-static tensile tests reported in Table 1, it can be hypothesized that the higher elastic modulus detected for the blend with a filler amount of 40 wt% leads to the application of a loading cycle with a lower deformation between the maximum and the minimum loads, with a lower damage on the material.

Considering that the stiffness drop detected in fatigue tests is directly related to the damage evolution within the material, it could be important to analyze the trend of the elastic modulus (normalized for the value detected in quasi-static conditions) as a function of the testing cycles for different stress levels. Normalized elastic modulus values for neat TPU and relative blends are thus reported in Figure 7(a–c). As it could be expected, a progressive decrease of the elastic modulus with the fatigue cycles can be seen at all the stress levels, regardless to the applied stress and to the presence of the capsules within the material. It is also clear that the decrease of the stiffness is more evident at elevated stress levels, while for applied stress equal to 0.3 σ_b the observed stiffness drop is rather limited, especially in the blend samples. According to the hysteresis loops shown in Figure 5, it is interesting to notice that an important drop of the material stiffness occurs even after the first testing cycle, especially at stress levels higher than 0.5 σ_b. It could be hypothesized that the interfacial debonding between TPU and the capsules occurs just after the application of the first fatigue cycle, and this could lead to a strong deterioration of the material resistance. But the modulus drop is observed also in the neat TPU samples, and this probably means that the fatigue damage occurs preferentially in the TPU matrix rather than at the interface. However, further microstructural analyzes will be performed in the future to have a better comprehension of this aspect.

The evolution of the damage within the samples can be observed also analyzing the trend of the absorbed energy as a function of the testing cycles for different fatigue stress levels. In Figure 8(a–c) the evolution of the absorbed energy (normalized for the energy absorbed in the first fatigue cycle) for the neat TPU and of the relative blend is reported. Once again, a strong drop of the absorbed energy could be observed in the first stages of the fatigue tests, while for higher testing cycles a certain stabilization occurs. It is also interesting to notice that this drop is proportional to the fatigue stress for all the testes compositions.

It is now important to evaluate the retention of the TES capability of the samples after fatigue tests in tensile

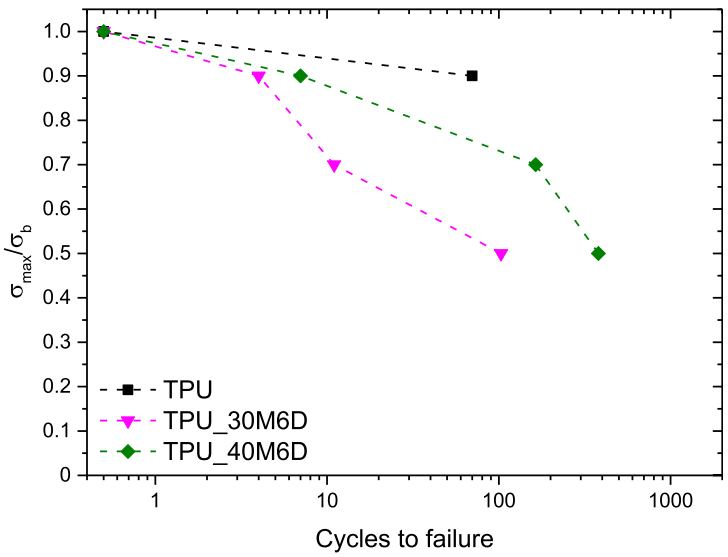

FIGURE 6 Wohler curves obtained from fatigue tests in tensile mode on the prepared blends. TPU, thermoplastic polyurethane [Color figure can be viewed at wileyonlinelibrary.com]

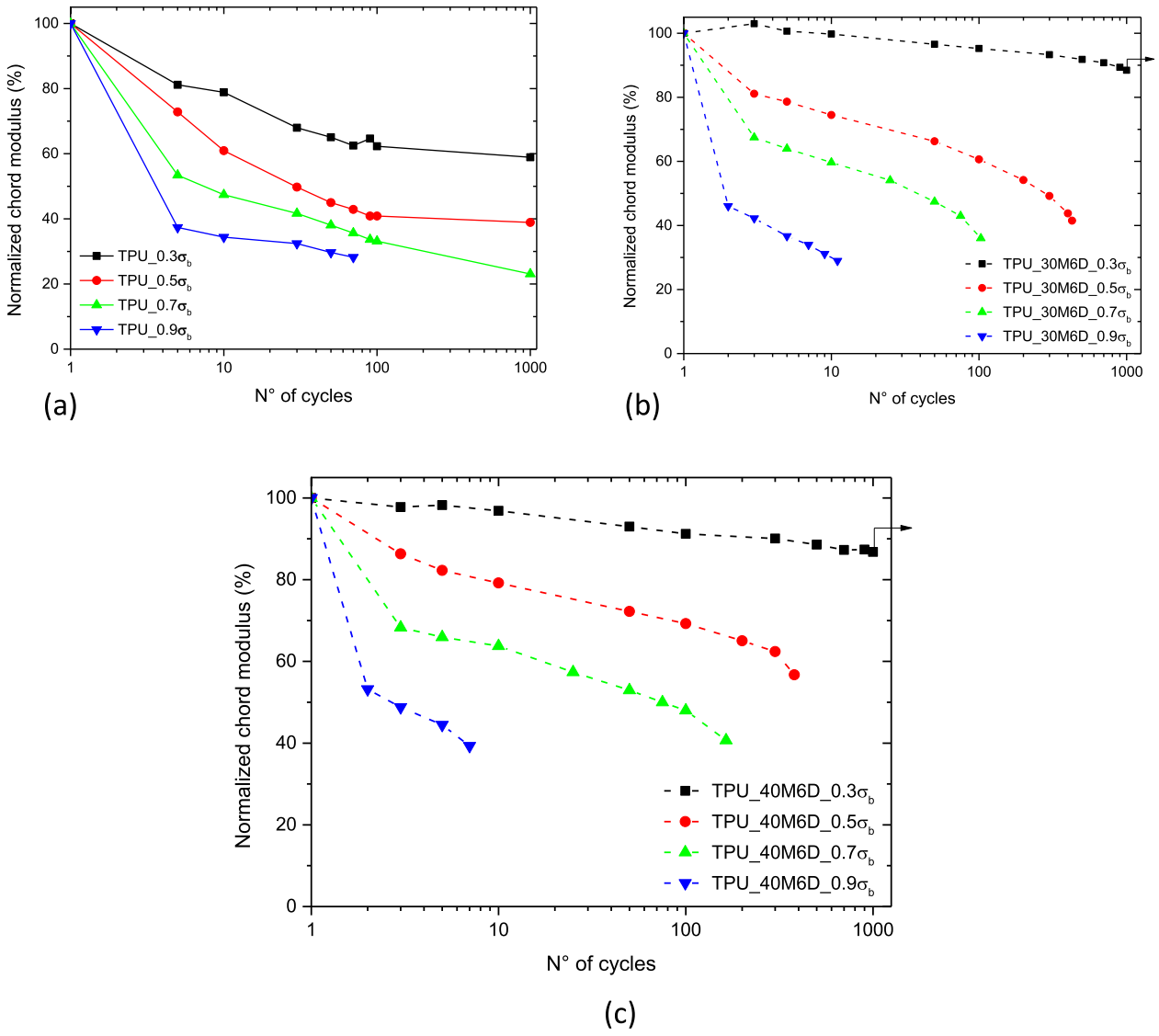

FIGURE 7 Evolution of the normalized chord modulus during fatigue tests in tensile mode on (a) TPU, (b) TPU_30M6D, and (c) TPU_40M6D samples. TPU, thermoplastic polyurethane [Color figure can be viewed at wileyonlinelibrary.com]

mode. In Table 2, the most important results of DSC on the prepared blends after fatigue tests are expressed in terms of specific melting (ΔH_m) and crystallization enthalpy (ΔH_c). Considering the experimental errors associated to these measurements, it is interesting to notice that for the TPU_30 M6D sample both ΔH_m and ΔH_c values remain fairly constant (i.e., around 23 J/g), regardless to the fatigue stress. Moreover, the values do not change neither if the materials reach the failure. Also, for the TPU_40 M6D blend the TES capability is rather stable (i.e., around 50 J/g), and only a slight decrease can be observed for stress levels higher than 0.9 σ_b. It can be therefore concluded that the TES capability of the prepared materials is retained even after 1000 fatigue tests in tensile conditions, and this means that the structural integrity of the capsules is not negatively affected by the application of tensile fatigue loads. Only at an elevated M6D loading (40 wt%) and under harsh fatigue conditions a small decrease of the TES properties, probably correlated to the partial breakage of some microcapsules within the material, occurs. This result is very important considering the intended applications of this material as shock-absorbing layer in shoes, as the TES power of the produced insoles could be retained even under prolonged and intense fatigue loadings.

3.4 | Compression fatigue tests

Considering the possible application of the prepared materials as insoles for running shoes, it could be also important to evaluate their fatigue behavior under

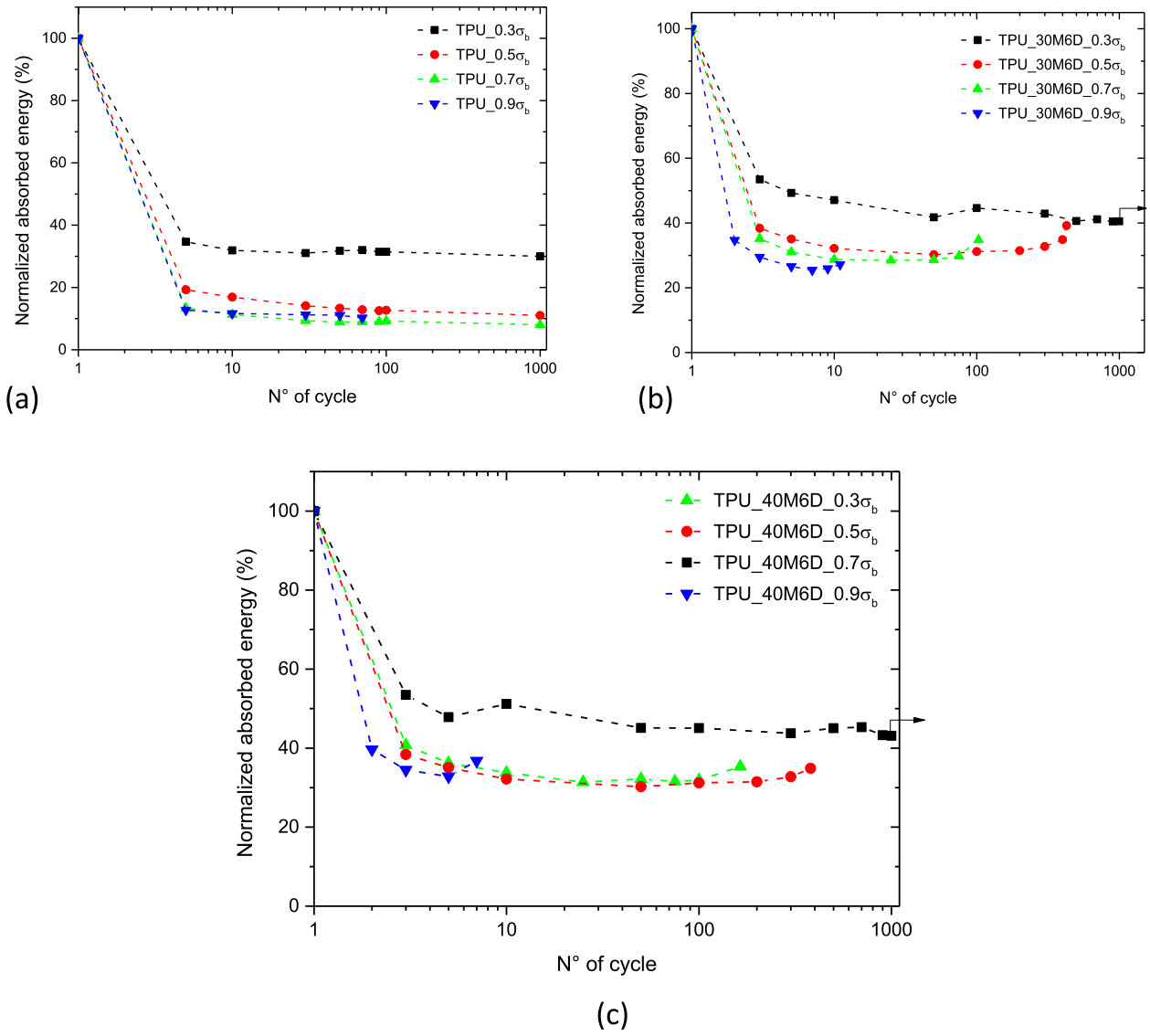

FIGURE 8 Evolution of the normalized energy absorbed in tensile fatigue tests on (a) TPU, (b) TPU_30M6D, and (c) TPU_40M6D samples. TPU, thermoplastic polyurethane [Color figure can be viewed at wileyonlinelibrary.com]

TABLE 2 Results of DSC tests on TPU_30 M6D and TPU_30 M6D samples after tensile fatigue tests

	σ_{max}/σ_b	N°cycle	Break (yes/no)	ΔH_m J/g	ΔH_c J/g
TPU_30M6D	0.3	1000	No	21.42	23.45
	0.5	427	Yes	27.23	27.26
	0.7	103	Yes	27.2	27.02
	0.9	11	Yes	22.88	22.62
	1.0	0.5	Yes	23.47	23.6
TPU_40M6D	0.3	1000	No	49.12	53.34
	0.5	380	Yes	49.49	49.82
	0.7	164	Yes	50.58	53.04
	0.9	7	Yes	44.97	46.39
	1.0	0.5	Yes	44.84	47.4

Abbreviations: DSC, differential scanning calorimetry; TPU, thermoplastic polyurethane.

compressive fatigue loadings. In Figure 9(a–d) hysteresis curves obtained from compressive fatigue tests on TPU_30 M6D and TPU_40MD6D samples at two different stress levels are reported. In accordance with quasi-static tensile tests reported in Table 1, it can be seen that even in compressive conditions the stiffness of the material is proportional to the capsules amount. It is also interesting to notice that, in accordance with the hysteresis curves obtained in tensile mode, the greatest part of the damage can be seen in the first fatigue loop. In fact, the amplitude of the hysteresis loop is more pronounced during the first fatigue cycle, especially if elevated stress levels (0.5 MPa) are applied to the material.

In order to have a deeper evaluation of the damage mechanisms under fatigue loadings, in Figure 10(a,b) the values of the normalized elastic modulus and of the normalized energy obtained from fatigue tests are respectively reported. It can be seen that the trend of the damage of the two tested samples is rather similar. If at a maximum compressive stress of 0.1 MPa the decrease in stiffness is not detectable, at elevated stress amplitude (i.e., 0.5 MPa) the drop of the elastic modulus is evident even after few fatigue cycles, and at 1000 cycles the stiffness of the two samples is about 10% of the pristine one. Considering the values of the normalized energy (Figure 10(b)), it can be concluded that the progressive damage evolution within the material determines a drop of the absorbed energy values. At a stress level of 0.5 MPa, the energy absorbed by the TPU_40M6D samples after 3 cycles is about the 42% of the pristine one, while after 1000 cycles it drops down to a value of about 20%. Even in this case, the capsules content does not seem to substantially influence the trend of the normalized energy. Once again, the stress level influences the energy absorbed by the materials. Increasing the maximum applied stress up to 0.5 MPa the specific energy values are systematically lower than those detected at 0.1 MPa, even after a limited number of fatigue cycles.

Finally, it is important to evaluate the retention of the TES capability even under compressive fatigue loadings. In Figure 11(a,b), the specific melting enthalpy values of the TPU_30M6D and TPU_40M6D samples obtained

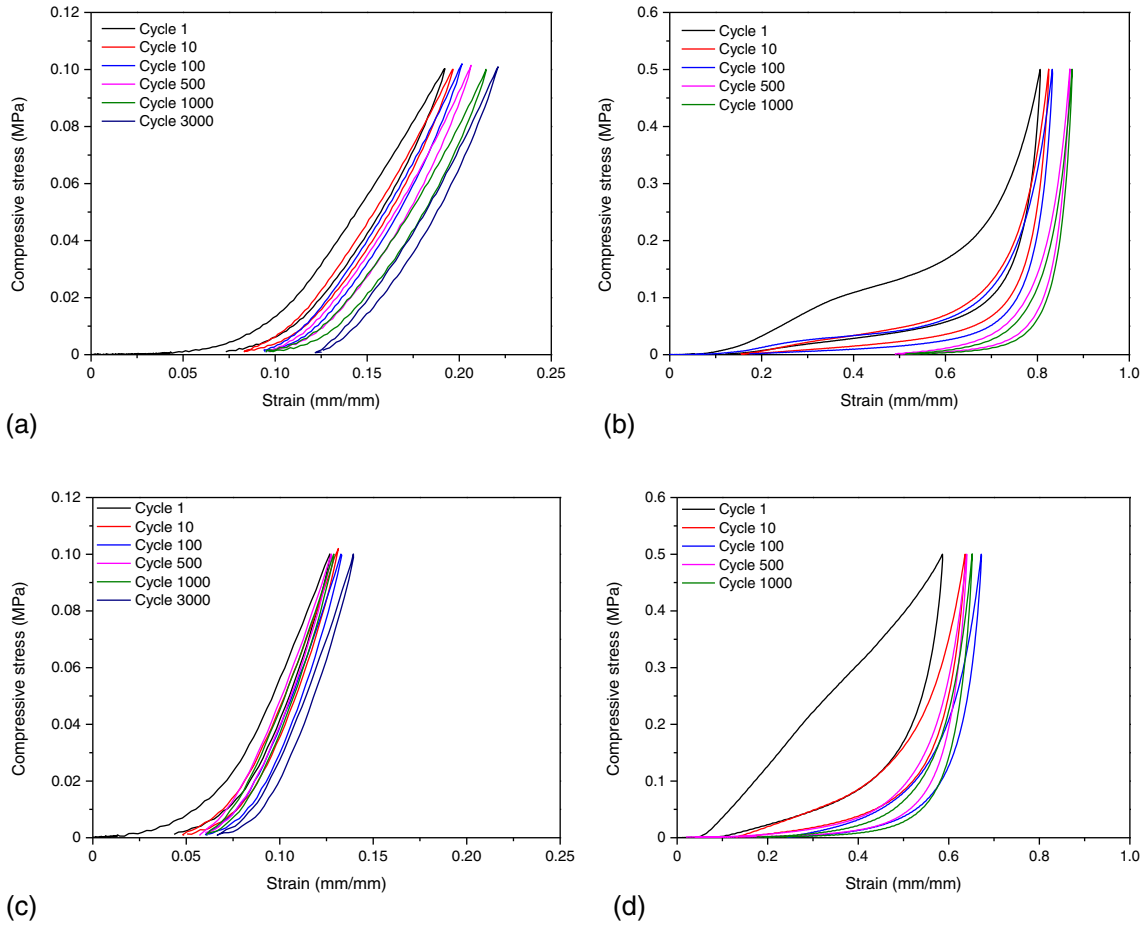

FIGURE 9 Hysteresis curves from compression fatigue tests on (a) TPU_30M6D (σ_{max} = 0.1 MPa), (b) TPU_30M6D (σ_{max} = 0.5 MPa), (c) TPU_40M6D (σ_{max} = 0.1 MPa), and (d) TPU_40M6D (σ_{max} = 0.5 MPa). TPU, thermoplastic polyurethane [Color figure can be viewed at wileyonlinelibrary.com]

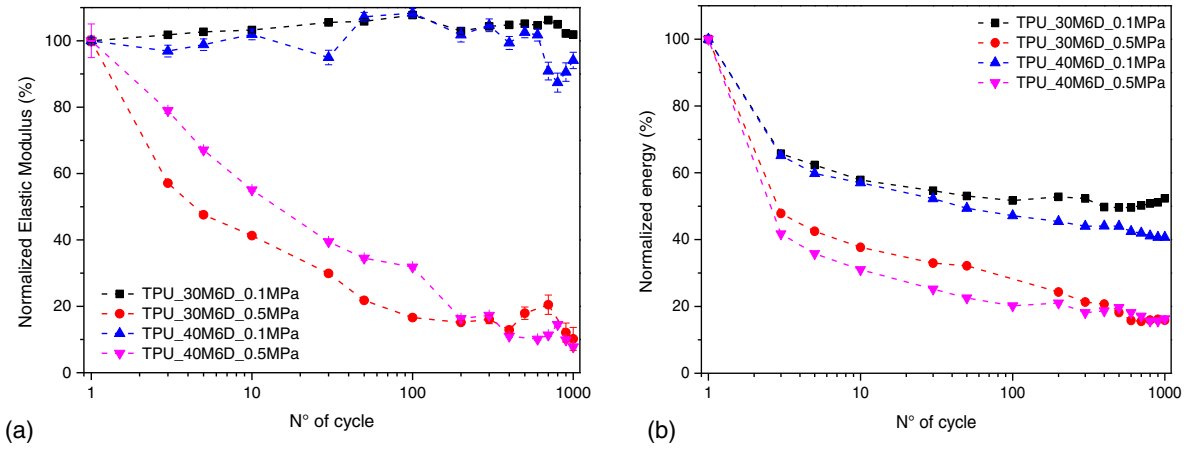

FIGURE 10 Evolution of (a) normalized elastic modulus and (b) normalized absorbed energy from compression fatigue tests on TPU_30M6D and TPU_40M6D samples. TPU, thermoplastic polyurethane [Color figure can be viewed at wileyonlinelibrary.com]

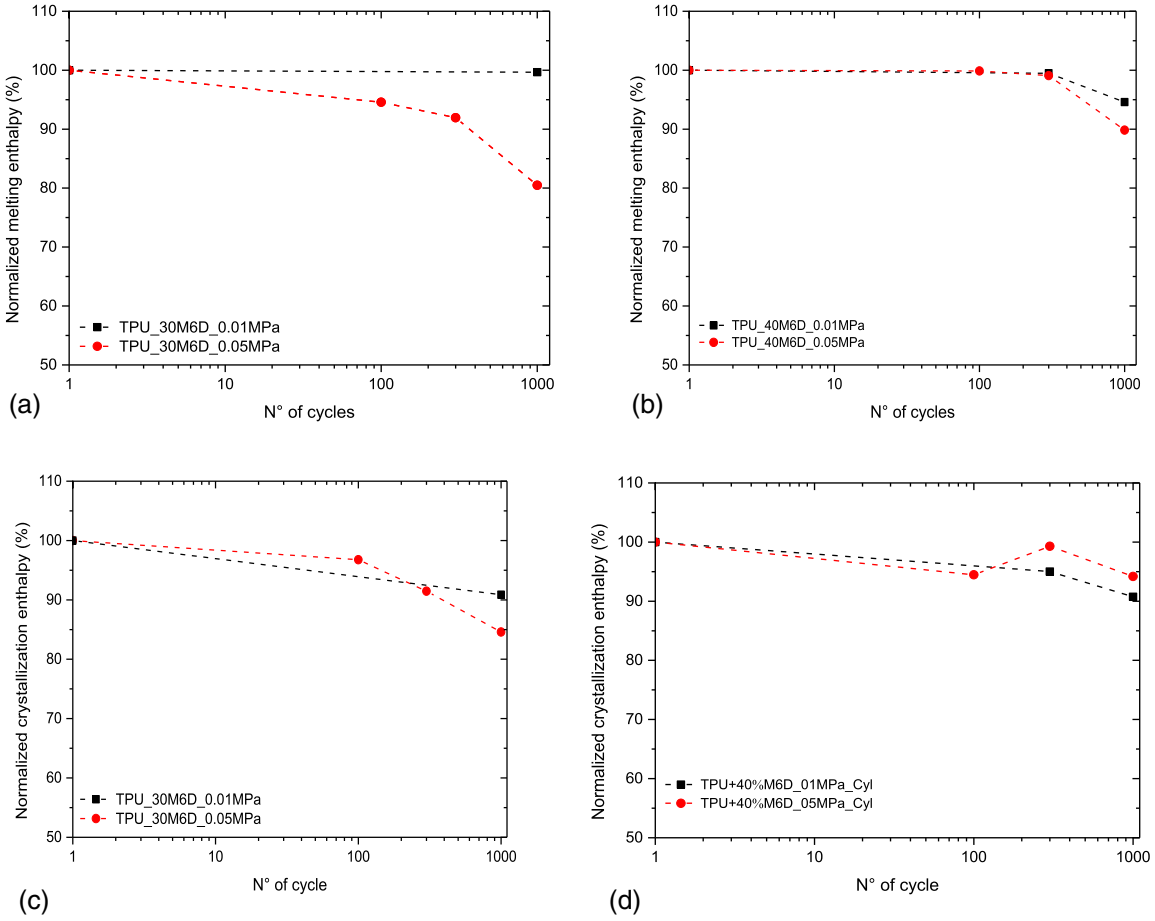

FIGURE 11 Evolution of the thermal energy capability of TPU/paraffin microcapsules blends from DSC tests on samples tested in compression fatigue mode. Normalized specific melting enthalpy values of (a) TPU_30M6D and (b) TPU_40M6D samples. Normalized specific crystallization enthalpy values of (c) TPU_30M6D and (d) TPU_40M6D samples. TPU, thermoplastic polyurethane [Color figure can be viewed at wileyonlinelibrary.com]

from DSC tests on specimens obtained from cylindric specimens at different fatigue cycles are respectively reported. In Figure 11(c–d), the corresponding crystallization enthalpy values are represented. It can be immediately seen that even in this case the capsules content does not affect the TES behavior of the prepared

samples, as the trends of both normalized ΔH_m and ΔH_c values is similar for TPU_30M6D and TPU_40M6D samples. It is interesting to notice that applying a maximum fatigue stress of 0.1 MPa the TES capability is not substantially decreased, and only a limited drop of both ΔH_m and ΔH_c can be detected after 1000 cycles. Even increasing the maximum applied stress up to 0.5 MPa the TES capability is not heavily compromised, neither after an elevated number of fatigue cycles. For instance, normalized ΔH_m value of the TPU_30M6D sample after 1000 cycles is about the 80% of the original one, while the normalized ΔH_c value is the 84% of the pristine one. In accordance to the results of DSC tests reported in Table 2, it can be concluded that the structural integrity of paraffin microcapsules is almost entirely retained even under compressive fatigue loadings, and the prepared materials maintain their TES capability even after an elevated number of fatigue cycles. Therefore, these results confirm the possibility to use these materials as insoles for running shoes and more in general for sport equipment applications.

4 | CONCLUSIONS

In this work, TPU/encapsulated paraffin blends to be applied as TES/release materials for sports applications were developed through a FDM technique and thermomechanically characterized. SEM analysis revealed a homogeneous distribution of the microcapsules within the matrix even at elevated M6D concentrations, associated to a rather good adhesion between the 3D printer layers. Quasi-static tensile test highlighted that the incorporation of microcapsules inside the matrix led to an important stiffening effect, accompanied by a heavy embrittlement of the material. Low-cycles fatigue tests, performed both in tensile and compressive mode, demonstrated that the introduction of M6D limited the fatigue life of 3D printed samples, and that a large part of the damage of the material took place during the first cycles. DSC analysis on the fatigue tested specimens revealed that the original TES properties of the samples were retained even at a relatively elevated (i.e., 1000) number of fatigue cycles, meaning that the structural integrity of the capsules was preserved and that the damage produced by the application of fatigue loading was probably localized within the matrix. It was therefore demonstrated the possibility to successfully use these multifunctional materials in applications in which the components are subjected to repeated stress, both in tensile and compressive mode.

ACKNOWLEDGMENTS

Mr. Massimiliano Casata and Mr. Emanuele Lodi are gratefully acknowledged for their support to the experimental work. This research activity has been supported by Fondazione Cassa di Risparmio di Trento e Rovereto (CARITRO) within the project Bando Caritro 2018 Ricerca e sviluppo. The work was also supported by the National Interuniversity Consortium of Materials Science and Technology (INSTM).

ORCID

Daniele Rigotti https://orcid.org/0000-0002-2337-8669

REFERENCES

[1] R. V. Feehery Jr.., *Clin. Podiatr. Med. Surg.* **1986**, *3*, 649.
[2] N. J. Mills, in *Materials in Sports Equipment* (Ed: M. Jenkins), Sawston, Cambridge, UK, Woodhead Publishing, **2003**.
[3] B. M. Nigg, D. Stefanyshyn, G. Cole, P. Stergiou, J. Miller, *J. Biomech.* **2003**, *36*, 569.
[4] C. H. Chen, K. H. Tu, C. Liu, T. Y. Shiang, *Hum. Movement Sci.* **2014**, *38*, 163.
[5] K. Brückner, S. Odenwald, S. Schwanitz, J. Heidenfelder, T. Milani, *Procedia. Eng.* **2010**, *2*, 2789.
[6] H. Mäkinen, K. Jussila, *Prot. Clothing* **2014**, *3*.
[7] C. Gao, K. Kuklane, I. Holmer, *Eur. J. Appl. Physiol.* **2011**, *111*, 1207.
[8] M. Itani, D. Ouahrani, N. Ghaddar, K. Ghali, W. Chakroun, *Build. Environ.* **2016**, *107*, 29.
[9] J. G. Drobny, *Handbook of Thermoplastic Elastomers*, Matthew Deans, Amsterdam, Netherlands, **2007**.
[10] J. A. Casado, F. Gutiérrez-Solana, I. Carrascal, S. Diego, J. A. Polanco, D. Hernández, *Compos. Part B* **2016**, *93*, 115.
[11] S. V. Susmita Bose, A. Bandyopadhyay, *Mater. Today* **2013**, *16*.
[12] U. Kalsoom, P. N. Nesterenko, B. Paull, *RSC Adv.* **2016**, *6*, 60355.
[13] G. Kim, E. Barocio, R. B. Pipes, R. Sterkenburg, *Addit. Manuf.* **2019**, *29*, 100809.
[14] H. Bi, Z. Ren, R. Guo, M. Xu, Y. Song, *Ind. Crops Prod.* **2018**, *122*, 76.
[15] A. Haryńska, J. Kucinska-Lipka, A. Sulowska, I. Gubanska, M. Kostrzewa, H. Janik, *Materials* **2019**, *12*, 887.
[16] S. S. Banerjee, S. Burbine, N. Kodihalli Shivaprakash, J. Mead, *Polymer* **2019**, *11*, 347.
[17] J.-Y. Lee, J. An, C. K. Chu, *Appl. Mater. Today* **2017**, *7*, 120.
[18] G. Gomez-Gras, R. Jerez-Mesa, J. A. Travieso-Rodriguez, J. Lluma-Fuentes, *Mater. Des.* **2018**, *140*, 278.
[19] J. M. Puigoriol-Forcada, A. Alsina, A. G. Salazar-Martín, G. Gomez-Gras, M. A. Pérez, *Mater. Des.* **2018**, *155*, 414.
[20] F. S. Senatov, K. V. Niaza, A. A. Stepashkin, S. D. Kaloshkin, *Compos. Part B* **2016**, *97*, 193.
[21] C. W. Ziemian, R. D. Ziemian, K. V. Haile, *Mater. Des.* **2016**, *109*, 209.
[22] M. M. Farid, A. M. Khudhair, S. A. K. Razack, S. Al-Hallaj, *Energy Convers. Manage.* **2004**, *45*, 1597.
[23] H. Shim, E. A. McCullough, B. W. Jones, *Text. Res. J.* **2016**, *71*, 495.
[24] A. Dorigato, P. Canclini, S. H. Unterberger, A. Pegoretti, *Express Polym. Lett.* **2017**, *11*, 738.
[25] A. Dorigato, M. V. Ciampolillo, A. Cataldi, M. Bersani, A. Pegoretti, *Rubber Chem. Technol.* **2017**, *90*, 575.
[26] G. Fredi, A. Dorigato, L. Fambri, A. Pegoretti, *Polymer* **2017**, *9*, 405.

[27] S. Sari-Bey, M. Fois, I. Krupa, L. Ibos, B. Benyoucef, Y. Candau, *Energy Convers. Manage.* **2014**, *78*, 796.
[28] X. Jin, J. Li, P. Xue, M. Jia, *Sol. Energy Mater. Sol. Cells* **2014**, *130*, 435.
[29] G. Fredi, A. Dorigato, L. Fambri, A. Pegoretti, *Compos. Sci. Technol.* **2018**, *158*, 101.
[30] A. Dorigato, G. Fredi, A. Pegoretti, *Front. Mater.* **2019**, *6*, 76.
[31] A. Dorigato, G. Fredi, A. Pegoretti, *J. Appl. Polym. Sci.* **2019**, *136*, 47434.
[32] G. Fredi, A. Dorigato, A. Pegoretti, *Polym. Compos.* **2019**, *40*, 3711.
[33] G. Fredi, A. Dorigato, A. Pegoretti, *Express Polym. Lett.* **2018**, *12*, 349.
[34] G. Fredi, A. Dorigato, S. Unterberger, N. Artuso, A. Pegoretti, *J. Appl. Polym. Sci.* **2019**, *136*, 47408.
[35] T. Khadiran, M. Z. Hussein, Z. Zainal, R. Rusli, *Sol. Energy Mater. Sol. Cells* **2015**, *143*, 78.
[36] H. Cao, *Active Coatings for Smart Textiles*, Woodhead Publishing, Sawston, UK, Cambridge, **2016**, p. 375.
[37] A. Dorigato, D. Rigotti, A. Pegoretti, *Front. Mater.* **2018**, *5*.
[38] D. Rigotti, A. Dorigato, A. Pegoretti, *Mater. Today Commun.* **2018**, *15*, 228.
[39] S. S. Zulkifli, W. P. Loh, *Foot Ankle Surg.* **2020**, *26*, 25.
[40] J. C. Halpin, *J. Compos. Mater.* **1969**, *3*, 732.

How to cite this article: Rigotti D, Dorigato A, Pegoretti A. Low-cycle fatigue behavior of flexible 3D printed thermoplastic polyurethane blends for thermal energy storage/release applications. *J Appl Polym Sci*. 2021;138:e49704. https://doi.org/10.1002/app.49704